Transparent uniaxial anisotropic spherical particles designed using radial anisotropy

Hui-Zhe Liu[*]
Department of Electrical and Computer Engineering, National University of Singapore, Singapore 119260

Joshua Le-Wei Li[†]
Institute of Electromagnetics and School of Electronic Engineering, University of Electronic Science and Technology of China, Chengdu, China 611731

Mook Seng Leong
Department of Electrical and Computer Engineering, National University of Singapore, Singapore 119260

Saïd Zouhdi
Laboratoire de Génie Electrique de Paris LGEP-Supélec, Plateau de Moulon, F-91192 Gif-sur-Yvette, France
(Received 25 December 2010; published 18 July 2011)

Based on Mie scattering theory and the assumption that the particle is electrically small in size ($k_t a \ll 1, k_m a \ll 1$), an analytic relationship between radial and tangential permittivity parameters has been established for achieving minimal scattering from an arbitrary rotationally uniaxial anisotropic spherical object incident by a plane wave. Analysis of fields in both the far- and near-field zones indicates that the derived relation is not only valid for electrically small particles, but also applicable to larger ones whose sizes are comparable with the free space wavelength after slight adjustments in parameters. Furthermore, it is observed that the dielectric spherical particle of reduced tangential permittivity yields better transparency performance than the design using a plasmonic cover by Alu and Engheta [Phys. Rev. E **72**, 016623 (2005)]. As such, particles with carefully engineered radial anisotropy are transparent without using any coating and are ideal for applications with space constraint and stringent transparency criteria.

DOI: 10.1103/PhysRevE.84.016605 PACS number(s): 41.20.−q, 42.25.Fx, 42.25.Bs

I. INTRODUCTION

During 1940s, research on invisibility was initiated for military purposes to hide aircraft from radar detection via stealth technology such as absorbent paint or purpose shaping. Later on, the concept of nonabsorbing coating of invisibility was envisioned in the research community [1]. In recent years, the interest in invisibility has revived as a result of advances in metamaterials. Unlike stealth technology where the incident power is either converted to heat or reflected in other directions, the usage of metamaterials opens up the possibility of preserving both the magnitude and direction of the incoming power flow. Moreover, potential applications of invisibility have spread to various engineering aspects, for instance, in medical probing and imaging.

Several ingenious approaches have been devised for the design of metamaterial coatings of invisibility, among which the two most popular ones are developed according to transformation optics [2–5] and scattering cancellation [1,6–8] techniques, respectively. The former approach is mathematically elegant in a sense that the designed coating is independent of the object to be hidden. On the other hand, this approach is practically challenging, and it requires materials to be both inhomogeneous and anisotropic. Methods have been proposed to reduce the material complexity of the transformation cloak by means of confining inhomogeneity to the radial direction [9–11] or forcing relative permeability to unity [12]. The latter approach, utilizing scattering cancellation technique, is ideal for electrically small particles where the higher-order contributions to the scattered fields are negligible. Furthermore, the coating is readily realizable by plasmonic materials such as noble metals at their plasma frequencies. In this work, the scattering cancellation approach is adopted for its ease of implementation.

In contrast to previously discussed cases where the employment of metamaterial coatings is necessary, we aim to design a spherical particle which is made transparent by the introduction of radial anisotropy. This work is inspired by the recent progress on the analysis and characterization of electromagnetic scattering by rotationally uniaxial anisotropic spheres. Based on full-wave Mie scattering theory, field solutions for scattering from anisotropic spheres can be analytically derived by a myriad of techniques, such as the expansion of spherical vector wave functions [13] or the introduction of Debye potentials [14,15] or novel potentials [16,17]. In particular, Debye potentials are utilized in this work. Previously, parametric analysis in the far-field zone has been carried out to study the effects of anisotropy on scattering by single spheres, be that diminution or enhancement [17,18]. As an extension, in this paper, an exact analytic relation in terms of constitutive parameters has been established for minimal scattering from rotationally uniaxial anisotropic spheres. Full-wave numerical analysis has been performed to validate the transparency relation in both the far- and near-field zones. In particular, effectiveness of the proposed design with reduced tangential or radial permittivity, in terms of scattered

[*]Also at Laboratoire de Génie Electrique de Paris LGEP-Supélec, Plateau de Moulon, F-91192 Gif-sur-Yvette, France.
[†]Corresponding author: lwli@ieee.org

fields and time-averaged Poynting vector distributions, has been compared against the former coated design in the near-field zone. With regard to its realizability, several designs of artificial radial anisotropy have been reported, such as media embedded with metal wires [19], multishell fullerene with central cavity [20], composites containing graded fibers [21], and thin layers with alternating permittivity [22,23].

In this paper, we extend the scattering cancellation technique to the case of rotationally uniaxial anisotropic spheres to minimize scattering. Following the theoretical formulation of fields with Debye potentials, we derive the transparency relation for zero scattering of rotationally uniaxial anisotropic spherical particles. In the long wavelength limit, we take one step further to examine the dipolar scattering coefficient and reach an expression of the effective permittivity of rotationally uniaxial anisotropic spheres. Last but not least, results from the full-wave numerical analysis are presented to validate the derived transparency relation and to demonstrate the effectiveness of the proposed designs in comparison to former design by Alu and Engheta [6].

II. THEORETICAL ANALYSIS

A. Theoretical background

In this paper, the interaction between electromagnetic waves and the spherical scatterer is formulated based on the Mie scattering model extended to the case of rotationally uniaxial anisotropic materials. The configuration of the problem is shown in Fig. 1. A rotationally uniaxial anisotropic spherical scatterer of radius a is centered at origin o and immersed in an isotropic host medium whose permittivity and permeability are denoted by ε_m and μ_m, respectively. An x-polarized monochromatic plane wave with unit amplitude travels along the z direction, given by

$$\boldsymbol{E}^i = \hat{\boldsymbol{x}} e^{ik_m z} e^{-i\omega t}, \tag{1}$$

where $k_m = \omega\sqrt{\varepsilon_m \mu_m}$. It should be noted that $e^{-i\omega t}$ is the implicit time-dependent factor and is suppressed in subsequent formulations without affecting any results. The permittivity and permeability tensors of the scatterer are defined in the spherical coordinates as $\bar{\boldsymbol{\varepsilon}} = (\varepsilon_r - \varepsilon_t)\,\hat{\boldsymbol{r}}\hat{\boldsymbol{r}} + \varepsilon_t \bar{\boldsymbol{I}}$ and $\bar{\boldsymbol{\mu}} = (\mu_r - \mu_t)\,\hat{\boldsymbol{r}}\hat{\boldsymbol{r}} + \mu_t \bar{\boldsymbol{I}}$, where the identity tensor is defined as $\bar{\boldsymbol{I}} = \hat{\boldsymbol{r}}\hat{\boldsymbol{r}} + \hat{\boldsymbol{\theta}}\hat{\boldsymbol{\theta}} + \hat{\boldsymbol{\phi}}\hat{\boldsymbol{\phi}}$, ε_r (μ_r) is the radial component of permittivity (permeability) along the $\hat{r}$ direction, and ε_t (μ_t) is the tangential component of permittivity (permeability) along the direction that is perpendicular to the $\hat{r}$ direction. It should be noted that $k_t = \omega\sqrt{\varepsilon_t \mu_t}$.

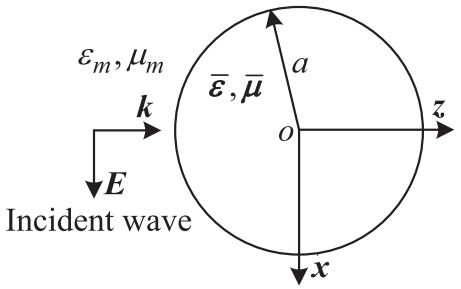

FIG. 1. Configuration of a scattering of incident plane wave by a rotationally uniaxial anisotropic spherical scatterer.

The incident wave described by Eq. (1) can be expanded in terms of spherical harmonics. In particular, the radial component of the incident electric field is given by

$$E_r^i = \frac{\cos\phi}{(k_m r)^2} \sum_{n=1}^{\infty} i^{n+1} (2n+1)\, \hat{J}_n (k_m r)\, P_n^{(1)} (\cos\theta), \tag{2}$$

where $\hat{J}_n(z)$ denotes the nth-order Riccati-Bessel function of the first kind; $P_n^{(1)}(\cos\theta)$ denotes the first-order associated Legendre function of degree n. An important relationship is given by $\hat{B}_n(z) = \sqrt{\pi z/2} B_{n+1/2}(z)$, where $\hat{B}_n$ represents the nth-order Riccati-Bessel functions of the first, second, and third kinds, namely, $\hat{J}_n$, $\hat{Y}_n$, $\hat{H}_n^{(1)}$; $B_{n+1/2}$ represents the pertinent $(n+1/2)$th-order cylindrical Bessel functions, namely, $J_{n+1/2}$, $Y_{n+1/2}$, and $H_{n+1/2}^{(1)}$, whose definitions are available in standard texts [24]. $P_n^{(1)}(\cos\theta)$ is related to the Legendre function of degree n, $P_n(\cos\theta)$, by $d P_n(\cos\theta)/d\theta = P_n^{(1)}(\cos\theta)$. All special functions mentioned in this paper strictly follow the definitions in [24].

For the convenience of matching boundary conditions along the spherical surface, we decouple the fields into transverse magnetic (TM) and transverse electric (TE) modes with respect to the $\hat{r}$ direction, which can be derived from the scalar TM and TE Debye potentials [15], Π^{TM} and Π^{TE}, respectively. Subsequently, we focus on results for TM mode only, since pertinent results for the TE mode can be conveniently derived by duality.

By following similar procedures presented in [15], the radial components of the incident, scattered and transmitted electric fields can be derived, with the introduction of appropriate Debye potentials, as

$$E_r^i = \left(\frac{\partial^2}{\partial r^2} + k_m^2\right)\left(r\Pi_i^{\mathrm{TM}}\right), \tag{3}$$

$$E_r^s = \left(\frac{\partial^2}{\partial r^2} + k_m^2\right)\left(r\Pi_s^{\mathrm{TM}}\right), \tag{4}$$

$$E_r^{\mathrm{obj}} = \left(\frac{\partial^2}{\partial r^2} + k_t^2\right)\left(r\Pi_{\mathrm{obj}}^{\mathrm{TM}}\right). \tag{5}$$

After making comparisons between the two expressions of E_r^i in Eqs. (2) and (3), the TM Debye potential for the incident field can by derived as

$$r\Pi_i^{\mathrm{TM}} = \frac{\cos\phi}{k_m^2} \sum_{n=1}^{\infty} \frac{i^{n+1}(2n+1)}{n(n+1)} \hat{J}_n(k_m r) P_n^{(1)}(\cos\theta). \tag{6}$$

Furthermore, the TM Debye potentials for the scattered and transmitted fields can be expressed as

$$r\Pi_s^{\mathrm{TM}} = -\frac{\cos\phi}{k_m^2} \sum_{n=1}^{\infty} T_n^{\mathrm{TM}} \frac{i^{n+1}(2n+1)}{n(n+1)} \times \hat{H}_n^{(1)}(k_m r)\, P_n^{(1)}(\cos\theta), \tag{7}$$

$$r\Pi_{\mathrm{obj}}^{\mathrm{TM}} = -\frac{\cos\phi}{k_t^2} \sum_{n=1}^{\infty} c_n^{\mathrm{TM}} \frac{i^{n+1}(2n+1)}{n(n+1)} \times \hat{J}_{v_n^{\mathrm{TM}}}(k_t r)\, P_n^{(1)}(\cos\theta), \tag{8}$$

where T_n^{TM} denotes the nth-order TM scattering coefficient, c_n^{TM} denotes the nth-order coefficient of the transmitted TM wave within the spherical object, $\hat{J}_{v_n^{\mathrm{TM}}}$ denotes the v_n^{TM}th-order Riccati-Bessel function of the first kind with

$$v_n^{\mathrm{TM}} = \sqrt{\frac{\varepsilon_t}{\varepsilon_r} n(n+1) + \frac{1}{4}} - \frac{1}{2}. \tag{9}$$

By matching boundary conditions at $r = a$ and solving the resultant linear equations, the nth-order TM scattering coefficient can be expressed as

$$T_n^{\mathrm{TM}} = \frac{C_n^{\mathrm{TM}}}{C_n^{\mathrm{TM}} + i D_n^{\mathrm{TM}}}, \tag{10}$$

where

$$C_n^{\mathrm{TM}} = \begin{vmatrix} \frac{\mu_t}{\mu_m}\hat{J}_n(k_m a) & \hat{J}_{v_n^{TM}}(k_t a) \\ \frac{k_t}{k_m}\hat{J}'_n(k_m a) & \hat{J}'_{v_n^{TM}}(k_t a) \end{vmatrix}, \tag{11}$$

$$D_n^{\mathrm{TM}} = \begin{vmatrix} \frac{\mu_t}{\mu_m}\hat{Y}_n(k_m a) & \hat{J}_{v_n^{TM}}(k_t a) \\ \frac{k_t}{k_m}\hat{Y}'_n(k_m a) & \hat{J}'_{v_n^{TM}}(k_t a) \end{vmatrix}, \tag{12}$$

with the prime sign denoting the derivative with respect to the argument.

The total scattering cross section of the object is defined as the ratio of the time-averaged total scattered power to the time-averaged incident power, denoted by

$$\sigma_{\mathrm{T}} = \frac{2\pi}{k_m^2} \sum_{n=1}^{\infty} (2n+1)\left(\left|T_n^{\mathrm{TM}}\right|^2 + \left|T_n^{\mathrm{TE}}\right|^2\right). \tag{13}$$

B. Derivation of transparency relation

To achieve zero scattering with reference to Eq. (13), we need to nullify the scattering coefficients. Taking the TM mode as an example, it can be observed that T_n^{TM} diminishes as long as its numerator C_n^{TM} given in Eq. (11) goes to zero. With the assumption that the scatterer is electrically small ($k_m a \ll 1, k_t a \ll 1$), the closed form expression of C_n^{TM} can be worked out as follows.

First, limiting values of Riccati-Bessel functions with small arguments can be expressed with reference to pertinent expressions of cylindrical Bessel functions [24] as

$$\hat{J}_v(k_m a) = \sqrt{\pi}(k_m/a\ 2)^{v+1}/\Gamma(v + 3/2), \tag{14}$$

$$\hat{Y}_v(k_m a) = -\sqrt{1/\pi}\,\Gamma(v + 1/2)(k_m a/2)^{-v}, \tag{15}$$

where $\Gamma(\cdot)$ denotes gamma function [24] and $\mathrm{Re}(v) > 0$.

By substituting Eq. (14) into Eq. (11), we then have

$$C_n^{\mathrm{TM}} = \frac{\pi}{2}\frac{\mu_t}{\mu_m}\frac{\left(\frac{k_m a}{2}\right)^{n+1}(k_t a 2)^{v_n^{\mathrm{TM}}}}{\Gamma\left(n+\frac{3}{2}\right)\Gamma\left(v_n^{\mathrm{TM}}+\frac{3}{2}\right)} \times \left[\left(v_n^{TM}+1\right) - \frac{\varepsilon_t}{\varepsilon_m}(n+1)\right]. \tag{16}$$

After setting $C_n^{\mathrm{TM}} = 0$ and substituting Eq. (9) into Eq. (16), we have

$$\frac{\varepsilon_t}{\varepsilon_m} = \frac{n + \frac{\varepsilon_r}{\varepsilon_m}}{(n+1)\frac{\varepsilon_r}{\varepsilon_m}}. \tag{17}$$

By duality, similar relation can be derived for nullifying the nth-order TE scattering coefficient as

$$\frac{\mu_t}{\mu_m} = \frac{n + \frac{\mu_r}{\mu_m}}{(n+1)\frac{\mu_r}{\mu_m}}. \tag{18}$$

For scattered fields by electrically small particles, the electric dipolar contribution (corresponding to $n = 1$) dominates and higher-order contributions become negligible in the summation in Eq. (13). Thus, the transparency relation with canceled electric dipole is derived from Eq. (17) as

$$\frac{\varepsilon_t}{\varepsilon_m} = \frac{1}{2}\frac{\varepsilon_m}{\varepsilon_r} + \frac{1}{2}. \tag{19}$$

Furthermore, we presume the scatterer is nonmagnetic (i.e., $\mu_r = \mu_t = \mu_0$). As such, Eq. (18) is always satisfied. In other words, the TE scattering coefficient in the present case is always negligible for small particles. When magnetic materials of the concerned scattering are considered, however, Eq. (18) will play an important role in the wave characterizations.

With reference to Eqs. (14) and (15), the electric dipolar scattering coefficient can be simplified from Eqs. (10)–(12) in the quasistatic limit as

$$T_1^{\mathrm{TM}} = -\frac{1}{3i}(k_m a)^3 \frac{\frac{2\varepsilon_t}{v_1^{\mathrm{TM}}+1} - \varepsilon_m}{\frac{\varepsilon_t}{v_1^{\mathrm{TM}}+1} + \varepsilon_m}. \tag{20}$$

As shown by Eq. (20), contributions of the tangential and radial components of permittivity to the dipolar scattering cannot be decoupled into two independent entities. Therefore, it can be inferred that the total dipole moment, in this case, is not a simple superposition of isolated contributions of tangential and radial components of permittivity. Coupling effect plays an important role. The above analysis provides physical insight into the parametric analysis of the electric and magnetic anisotropy in [17].

When the sphere is isotropic with $\varepsilon_t = \varepsilon_r = \varepsilon_s$, Eq. (20) is reduced to the Rayleigh scattering case as

$$T_1^{\mathrm{TM}} = -\frac{2}{3i}(k_m a)^3 \frac{\varepsilon_s - \varepsilon_m}{\varepsilon_s + 2\varepsilon_m}. \tag{21}$$

By making comparisons between Eq. (20) and (21), we arrive at an expression of effective permittivity of the anisotropic sphere as

$$\varepsilon_s = \frac{2\varepsilon_t}{v_1^{\mathrm{TM}} + 1}, \tag{22}$$

which was derived independently for the first time when this paper was finished, to our knowledge. However, it was known that the same expression was independently obtained, expressed in a different form, and published in another paper slightly later in [25]. Equation (22) is particularly useful for future analysis of composite medium embedded with rotationally uniaxial anisotropic inclusions. It can be inferred from Eq. (22) that the effective permittivity of the particle ε_s is always equal to that of the surrounding medium ε_m, when the transparency relation given by Eq. (19) is satisfied. This observation coins with the "neutral inclusion" concept developed for the design of transparent particles in [26].

III. NUMERICAL ANALYSIS

A. Far-field analysis

With the introduction of radial anisotropy, we attempt to suppress the electric dipolar term T_1^{TM}, which is the major contributor to wave scattering for an isotropic spherical particle. For instance, an isotropic sphere with $\varepsilon = 3\varepsilon_0$, $\mu = \mu_0$, and $a = \lambda_0/5$ yields normalized total scattering cross section of $\sigma_{\mathrm{T}}/\lambda_0^2 = 0.12$ where the dominant scattering coefficient $T_1^{\mathrm{TM}} = 0.47$ is about three times $T_1^{\mathrm{TE}} = 0.18$. In the following analysis, the total scattering cross section and first few scattering coefficients for three cases are examined, namely, for electrically small particle ($a = \lambda_0/100$) with varying ε_r and larger particle ($a = \lambda_0/5$) with either varying ε_r or varying ε_t. The host medium is presumed to be air with $\varepsilon_m = \varepsilon_0$ throughout this section.

To begin with, we set $\varepsilon_t = 3\varepsilon_0$ and $a = \lambda_0/100$. The normalized total scattering cross section $\sigma_{\mathrm{T}}/\lambda_0^2$ is examined over a range of $\varepsilon_r/\varepsilon_0$ in Fig. 2(a). The dip of the plot occurs at $\varepsilon_r/\varepsilon_0 = 0.2$, which is in perfect agreement with the previously derived transparency relation in Eq. (19). In Fig. 2(b), the contribution of the first-order TM scattering coefficient, T_1^{TM}, is plotted against $\varepsilon_r/\varepsilon_0$. The TE and higher-order TM scattering coefficients are not presented here since their magnitudes, being at least two orders lower than T_1^{TM}, are comparatively negligible. In this case, the electric dipolar term, T_1^{TM}, can thus be treated as the sole contributor to scattering. The minima of T_1^{TM} and $\sigma_{\mathrm{T}}/\lambda_0^2$ take place at the same $\varepsilon_r/\varepsilon_0$ value. As such, minimum scattering takes place due to the cancellation of the electric dipole depicted in Eq. (20).

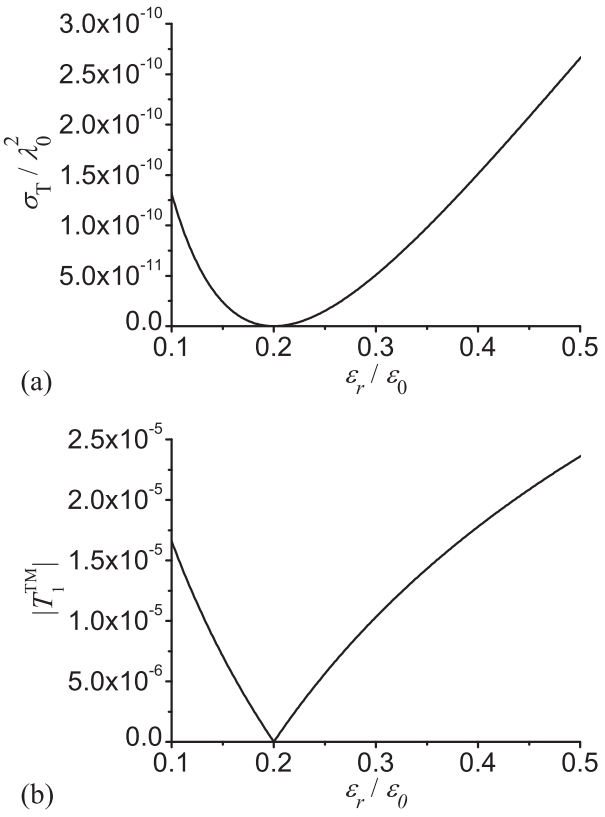

FIG. 2. (a) Normalized total scattering cross section and (b) contribution of the first-order TM scattering coefficient, with respect to $\varepsilon_r/\varepsilon_0$, with $\varepsilon_t = 3\varepsilon_0$, $\mu = \mu_0$, and $a = \lambda_0/100$.

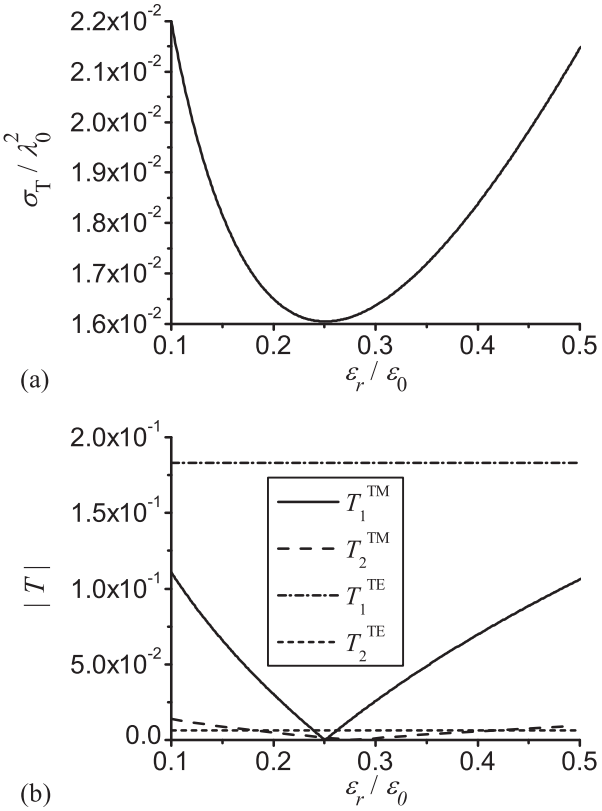

FIG. 3. (a) Normalized total scattering cross section and (b) contributions of several TM and TE scattering coefficients, with respect to $\varepsilon_r/\varepsilon_0$ with $\varepsilon_t = 3\varepsilon_0$, $\mu = \mu_0$, and $a = \lambda_0/5$.

At $a = \lambda_0/100$, the case with $\varepsilon_r = 3\varepsilon_0$ and varying ε_t yields a similar plot as in Fig. 2. The result is not shown here for the sake of brevity.

In Fig. 3, the particle has the same parameters as those in Fig. 2, except $a = \lambda_0/5$ instead of $\lambda_0/100$. In Fig. 3(a), the dip occurs at $\varepsilon_r/\varepsilon_0 = 0.25$, which is higher than in Fig. 2(a). As such, the transparency relation given by Eq. (19) requires slight adjustment in value. This is because as the object becomes larger, small-argument approximations to Riccati-Bessel functions are no longer appropriate. Therefore, the full expression in Eq. (11), instead of the simplified expression in Eq. (16), has to be equal to zero in order to cancel T_1^{TM}.

In Fig. 3(b), it can be observed that as the particles size increases, the contribution of the magnetic dipole T_1^{TE} is no longer negligible. T_1^{TE} is independent of ε_r and therefore has no effect on the position of the dip in Fig. 3(a). As such, the position of the minimum $\sigma_{\mathrm{T}}/\lambda_0^2$ is still determined by the minimum in T_1^{TM}. In other words, the minimum in scattering corresponds to the cancellation of electric dipole even when the particle size is comparable to the free space wavelength.

In Fig. 4, the object has the same parameters as those in Fig. 3, except that $\varepsilon_r = 3\varepsilon_0$ is held as constant instead of ε_t. In Fig. 4(a), the dip occurs at $\varepsilon_t/\varepsilon_0 = 0.62$, which is slightly lower than the predicted value of $\varepsilon_t/\varepsilon_0 = 0.67$ in Eq. (19). The position of the dip in Fig. 4(a) depends not only on the dip in electric dipole T_1^{TM} but also on values of magnetic dipole T_1^{TE}

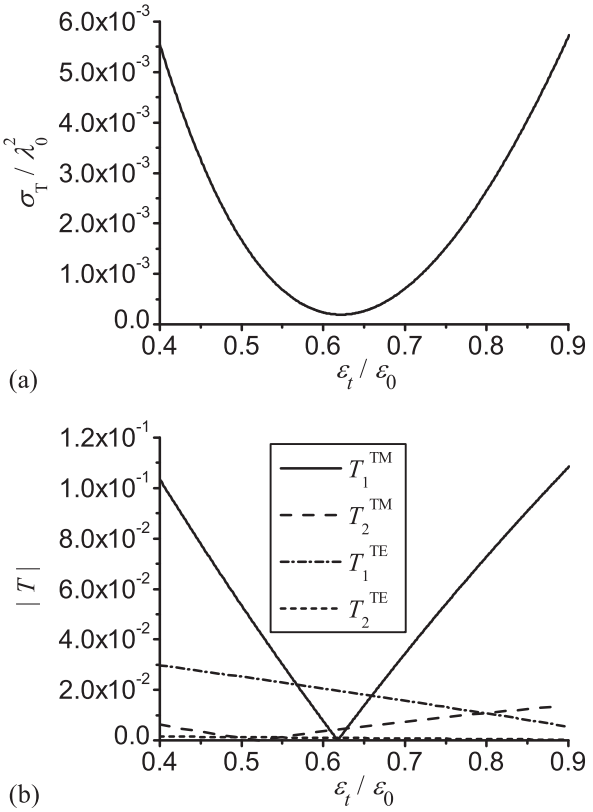

FIG. 4. (a) Normalized total scattering cross section and (b) contributions of several TM and TE scattering coefficients, with respect to $\varepsilon_t/\varepsilon_0$ with $\varepsilon_r = 3\varepsilon_0$, $\mu = \mu_0$, and $a = \lambda_0/5$.

and electric quadrupole T_2^{TM} since they all vary with changing ε_t, as shown in Fig. 4(b).

B. Near-field analysis

Among the six components of scattered fields, the radial electric field E_r^s is selected for demonstrating effects of canceling T_1^{TM}, since its expression solely depends on the TM Debye potential as shown in Eq. (4). Furthermore, the x-z plane, also termed as the E plane, is chosen for field plotting after inspecting Eq. (7). It is apparent that the TM Debye potential, as well as all of its multipolar terms, yield maximal values in the E plane where $\cos\phi = 1$.

Four cases are carefully examined. An isotropic sphere with $\varepsilon = 3\varepsilon_0$, $\mu = \mu_0$, and $a = \lambda_0/5$ is chosen as the reference scatterer in Fig. 5(a). Designed according to procedures proposed in [6], a coating layer with optimal parameters, $a_c = 1.49a$ and $\varepsilon_c = 0.5\varepsilon_0$, is placed around the reference sphere in Fig. 5(b). The last two cases are obtained by introducing optimal tangential or radial permittivity into the reference sphere. In Fig. 5(c), we have $\varepsilon_t = 3\varepsilon_0$ and $\varepsilon_r = 0.25\varepsilon_0$; in Fig. 5(d) we have $\varepsilon_t = 0.62\varepsilon_0$ and $\varepsilon_r = 3\varepsilon_0$, corresponding to the optimal values observed at the dips in Figs. 3(a) and 4(a), respectively.

Figure 5(a) serves as the reference plot, displaying a dipolar pattern for the magnitude of the radial component of the scattered electric field $|E_r^s|$ in the E plane for an isotropic spherical particle. The rest of the contour plots in Fig. 5 manifest quadrupolar patterns signifying the successful cancellation

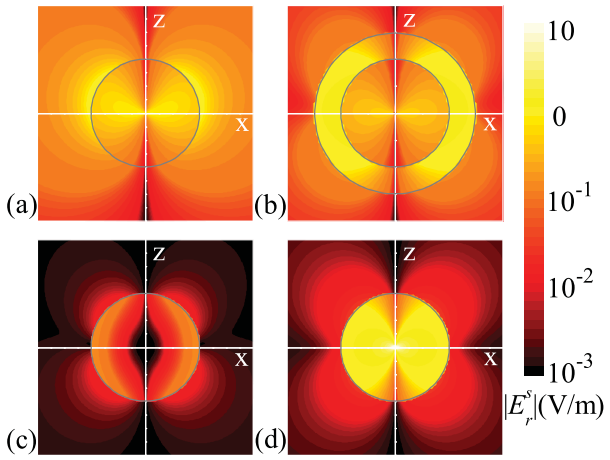

FIG. 5. (Color online) Contour plots of magnitudes of radial components of scattered electric fields in the x-z plane for (a) an isotropic sphere with $\varepsilon = 3\varepsilon_0$, $\mu = \mu_0$, and $a = \lambda_0/5$; (b) the same as (a), except for a coating of $a_c = 1.49a$ and $\varepsilon_c = 0.5\varepsilon_0$; (c) the same as (a), except that $\varepsilon_t = 3\varepsilon_0$ and $\varepsilon_r = 0.25\varepsilon_0$; and (d) the same as (a), except that $\varepsilon_t = 0.62\varepsilon_0$ and $\varepsilon_r = 3\varepsilon_0$.

of the electric dipolar contribution T_1^{TM} to scattering. Among the three quadrupolar patterns, Fig. 5(b) representing former work [6] depicts the highest scattering magnitude because the added coating layer increases the total volume of the scatterer and hence enhances higher-order contributions to scattering. The scattering pattern in Fig. 5(c) is the lowest in magnitude in agreement with the close-to-zero values of T_1^{TM} and T_2^{TM} as shown in Fig. 3(b) at the optimal point of $\varepsilon_r = 0.25\varepsilon_0$. In short, the two proposed designs yield better transparency performance in the TM mode than former work, in a sense that the magnitudes of the radial components of the scattered fields in Figs. 5(c) and 5(d) are about one order lower than that in Fig. 5(b).

Figure 6 shows the total time-averaged Poynting vector distribution in the E plane for the same setups as in Fig. 5. Figures 6(b)–6(d) display different degrees of reduced forward scattering as compared with Fig. 6(a). Figure 6(d) shows the best performance with nearly unperturbed power flow. This is because both the TM and the TE scattering coefficients of a dielectric sphere can be significantly reduced with the introduction of optimal ε_t value, as shown in modal analysis at $\varepsilon_t = 0.62\varepsilon_0$ in Fig. 4(b), which leads to negligible scattered power in Fig. 6(d). On the other hand, the forward scattering in Fig. 6(c) is not fully eliminated, despite of the low contribution from TM mode, as shown in Fig. 5(c), since its TE scattering coefficients are unabated by changing ε_r value, as shown in Fig. 3(b). Overall, the proposed design in Fig. 6(d) with negligible forward scattering demonstrates superior transparency performance over the one representing the former design in Fig. 6(b).

IV. CONCLUSIONS

In this paper, we have demonstrated that carefully engineered radial anisotropy, in an effort to cancel the dominant electric scattering coefficient T_1^{TM}, leads to remarkable reduction in scattering by a single dielectric sphere. A transparency

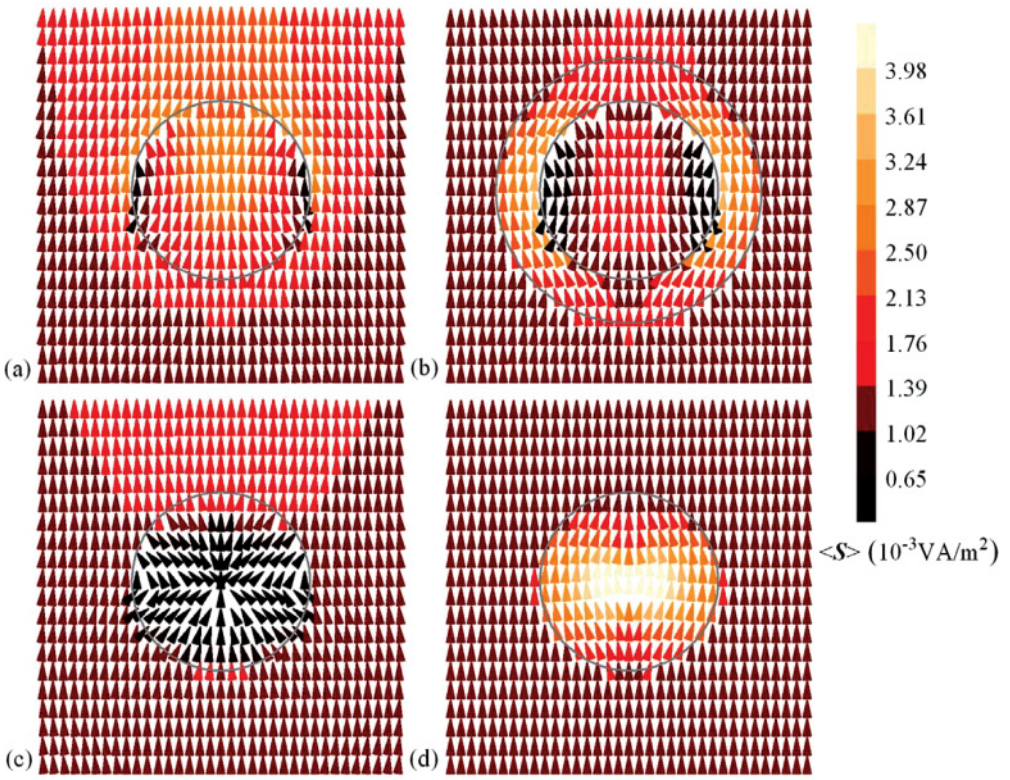

FIG. 6. (Color online) Total time-averaged Poynting vector distribution in the E plane for the same four cases as in Fig. 5.

relation between ε_r and ε_t has been analytically established based on the Mie theory which leads to the precise prediction of the optimal parameters for electrically small particles and requires slight adjustments with the increase in particle size. The design with optimized tangential permittivity gives the best transparency performance in a sense that that the power flow is almost unaffected by the presence of the object. On the other hand, the design with optimized radial permittivity can be improved by reducing contributions from its TE scattering coefficients with a suitable permeability, which can be a topic for future work.

Compared to previous coating designs, the designed single anisotropic sphere has its distinct merits. From an engineering point of view, it is more robust. For instance, in applications such as medical probing and imaging, this technique can be applied to design a robust probe without having to worry about the wear and tear of any additional coating layer whose performance depends on a fixed core-shell radial ratio [6,15]. In addition, the design with reduced tangential permittivity yields better transparency performance over the coated design, as shown in the near-field analysis. As such, the proposed design is useful for applications with space constraint, long durability, and stringent transparency criteria.

ACKNOWLEDGMENTS

The authors are grateful for the financial support to Huizhe Liu in terms of the Merlion Ph.D. program and the financial support to Professor Saïd Zouhdi in France and Professor Joshua Le-Wei Li in Singapore, both by the French Embassy in Singapore. Huizhe Liu also acknowledges the research support provided by National University of Singapore. Professor Joshua Le-Wei Li is grateful for the financial support by the University of Electronic Science and Technology of China, Chengdu, China under the China's 1000-Talent Scheme.

[1] M. Kerker, J. Opt. Soc. Am. **65**, 376 (1975).
[2] A. Greenleaf, M. Lassas, and G. Uhlmann, Math. Res. Lett. **10**, 685 (2003).
[3] J. B. Pendry, D. Schurig, and D. R. Smith, Science **312**, 1780 (2006).
[4] U. Leonhardt, Science **312**, 1777 (2006).
[5] U. Leonhardt and T. G. Philbin, *Geometry and Light: The Science of Invisibility* (Dover, Mineola, 2010).
[6] A. Alu and N. Engheta, Phys. Rev. E **72**, 016623 (2005).
[7] A. Alu and N. Engheta, Opt. Express **15**, 3318 (2007).
[8] A. Alù and N. Engheta, J. Opt. A: Pure Appl. Opt. **10**, 093002 (2008).
[9] S. A. Cummer, B. I. Popa, D. Schurig, D. R. Smith, and J. Pendry, Phys. Rev. E **74**, 036621 (2006).
[10] M. Yan, Z. Ruan, and M. Qiu, Opt. Express **15**, 17772 (2007).
[11] W. Yan, M. Yan, and W. Qiu, Appl. Phys. Lett. **93**, 021909 (2008).

[12] W. Cai, U. K. Chettiar, A. V. Kildishev, V. M. Shalaev, and G. W. Milton, Appl. Phys. Lett. **91**, 111105 (2007).
[13] Y.-L. Geng, X.-B. Wu, L.-W. Li, and B.-R. Guan, Phys. Rev. E **70**, 056609 (2004).
[14] M. Born and E. Wolf, *Principle of Optics: Electromagnetic Theory of Propagation Interference and Diffraction of Light*, 7th ed. (Cambridge Unviersity Press, Cambridge, 1999).
[15] L. Gao, T. H. Fung, K. W. Yu, and C. W. Qiu, Phys. Rev. E **78**, 046609 (2008).
[16] K. L. Wong and H. T. Chen, IEE Proc., Part H: Microwaves, Antennas Propag. **139**, 314 (1992).
[17] C.-W. Qiu, L.-W. Li, T.-S. Yeo, and S. Zouhdi, Phys. Rev. E **75**, 026609 (2007).
[18] B. S. Luk'Yanchuk and C.-W. Qiu, Appl. Phys. A **92**, 773 (2008).
[19] W. Cai, U. K. Chettiar, A. V. Kildishev, and V. M. Shalaev, Nat. Photon. **1**, 224 (2007).
[20] A. A. Lucas, L. Henrard, and P. Lambin, Phys. Rev. B **49**, 2888 (1994).
[21] G. Q. Gu and K. W. Yu, J. Compos. Mater. **39**, 127 (2005).
[22] Y. Huang, Y. Feng, and T. Jiang, Opt. Express **15**, 11133 (2007).
[23] C.-W. Qiu, L. Hu, X. Xu, and Y. Feng, Phys. Rev. E **79**, 047602 (2009).
[24] M. Abramowitz and I. A. Stegun, *Handbook of Mathematical Functions with Formulas, Graphs, and Mathematical Tables* (Dover, New York, 1965).
[25] Y. Ni, D. L. Gao, Z. F. Sang, L. Gao, and C. W. Qiu, Appl. Phys. A **102**, 673 (2011).
[26] X. Zhou and G. Hu, Phys. Rev. E **74**, 026607 (2006).